Chinese Chemical Letters 37 (2026) 112130

Contents lists available at ScienceDirect

Chinese Chemical Letters

journal homepage: www.elsevier.com/locate/cclet

Controlled shikonin delivery from polycaprolactone scaffolds promotes diabetic wound repair *via* coordinated inflammation resolution and angiogenesis

Zeyu Xu[a,b], Ming Zhang[a,b], Tangtang He[a,b], Zhe Wang[c], Wenwen Deng[c], Xia Cao[c], Qilong Wang[c], Yiwei Wang[a], Jun Chen[a,b,*]

[a] *School of Pharmacy, Nanjing University of Chinese Medicine, Nanjing 210023, China*
[b] *Jiangsu Provincial Engineering Research Center of TCM External Medication Development and Application, Nanjing University of Chinese Medicine, Nanjing 210023, China*
[c] *Department of Pharmaceutics, School of Pharmacy, Center for Nano Drug/Gene Delivery and Tissue Engineering, Jiangsu University, Zhenjiang 212013, China*

ARTICLE INFO

Article history:
Received 13 October 2025
Revised 14 November 2025
Accepted 17 November 2025
Available online 19 November 2025

Keywords:
Diabetic wound healing
Controlled drug release
Shikonin delivery
3D-printed scaffold
Anti-inflammatory therapy

ABSTRACT

Chronic diabetic wounds are characterized by persistent inflammation and impaired angiogenesis, presenting a major therapeutic challenge. Here, we report a three-dimensional (3D)-printed polycaprolactone (PCL) scaffold integrating shikonin (SK), a bioactive compound derived from *Lithospermum erythrorhizon*, to achieve controlled drug release and multifunctional wound repair. The PCL/SK scaffold exhibited a porous, breathable architecture with high mechanical integrity and biocompatibility, enabling sustained SK release over 72 h. In a diabetic mouse wound model, the PCL/SK scaffold significantly accelerated wound closure, enhanced collagen deposition, and increased the density of anti-inflammatory $CD206^+$ macrophages compared to free SK or PCL controls. Transcriptomic and immunohistochemical analyses revealed that PCL/SK treatment upregulated angiogenesis-related genes, including vascular endothelial growth factor (*Vegf*), platelet endothelial cell adhesion molecule 1 (*Pecam1*) and TEK receptor tyrosine kinase (*Tek*), meanwhile elevated $CD31^+$ and $VEGF^+$ endothelial markers, concomitant with improved blood perfusion. Mechanistically, this effect was attributed to synergistic anti-inflammatory and pro-angiogenic modulation by sustained SK delivery and the supportive PCL microenvironment. These findings establish a bioactive drug-biomaterial hybrid platform that leverages controlled release to coordinate immune resolution and vascular regeneration, offering a promising strategy for chronic diabetic wound management and broader regenerative applications.

© 2026 Published by Elsevier B.V. on behalf of Chinese Chemical Society and Institute of Materia Medica, Chinese Academy of Medical Sciences.

Diabetic wounds, which occur in 15 %–25 % of diabetic patients, are open sores or ulcers that are highly susceptible to chronic inflammation, oxidative stress, impaired angiogenesis, and increased infection risk [1,2]. These complications delay healing and elevate morbidity, rendering the management of diabetic wounds a significant clinical challenge [3,4]. Current therapeutic strategies encompass systemic and topical antibiotics [5], growth factors [6], traditional Chinese medicines (TCM) [7], and advanced wound dressings [8]. However, these treatments often fall short in comprehensively addressing the underlying pathophysiological mechanisms. Chronic inflammation is a key factor that exacerbates the complexity of diabetic wounds [9–11], and effective anti-inflammatory treatments are crucial for promoting healing.

Wound dressings have become an essential clinical therapy option, typically categorized into traditional types, such as gauze, and modern alternatives, like silver-based products (*e.g.*, Acticoat™, Actisorb®, and Silver Contreet) [12,13]. While silver-based dressings possess antimicrobial properties, their cytotoxicity may hinder fibroblast activity, which is vital for wound healing, thereby potentially slowing the overall healing process [13,14]. An ideal wound dressing should mitigate inflammation, prevent bacterial infection, and stimulate cell proliferation and tissue regeneration to meet long-term therapy demand [15]. Recent advances harness multifunctional scaffolds that integrate antimicrobial, antioxidant and pro-angiogenic cues to orchestrate timely healing of diabetic wounds. These bioactive constructs simultaneously provide a three-dimensional (3D) cell-instructive matrix, achieve sustained

* Corresponding author.
E-mail address: chenjun75@njucm.edu.cn (J. Chen).

https://doi.org/10.1016/j.cclet.2025.112130
1001-8417/© 2026 Published by Elsevier B.V. on behalf of Chinese Chemical Society and Institute of Materia Medica, Chinese Academy of Medical Sciences.

release of therapeutics, and counteract the chronic inflammation and oxidative stress inherent to diabetic lesions, thereby significantly accelerating closure. Polycaprolactone (PCL) is a widely used synthetic polymer for the construction of scaffolds [16,17] and extensively explored in biomedical applications, including in drug delivery [18], cancer treatment, bone regeneration engineering, and particularly skin wound healing [19], owing to its anti-inflammatory properties, capacity for sustained drug release, biodegradability, and high mechanical strength.

The blood-cooling properties of Zicao (*Lithospermum erythrorhizon*) are particularly relevant to the "heat toxin" manifestation associated with diabetes. Shikonin (SK), the main active compound in *Lithospermum erythrorhizon*, has been documented to facilitate wound healing [20,21]. In this study, we present scaffolds that integrate PCL with SK using 3D printing technology to enhance the healing efficacy of diabetic wounds. The resulting PCL/SK scaffolds possess several advantages, including biocompatibility and anti-inflammatory capabilities, and a porous, breathable structure that maintains a dry wound environment. These scaffolds are specifically designed to load and sustainably release SK, thereby jointly promoting wound healing. In a *db/db* mouse wound model, PCL/SK scaffolds demonstrate their therapeutic efficacy in promoting diabetic wound healing and elucidate their angiogenic mechanisms. This study aims to provide a novel therapeutic strategy for diabetic wound healing and offer valuable insights for the design and fabrication of multifunctional scaffolds.

The PCL/SK scaffold was fabricated using 3D printing. To investigate the effect of polymer concentration, the printing temperature and speed were fixed at 40 °C and 15 mm/s, respectively, while the polymer concentration was varied at 10 %, 20 %, and 25 % w/v. Scaffold pore uniformity was used as an indicator of structural formability. Increasing the PCL concentration significantly improved the uniformity of pore size distribution (Fig. 1a), with the best uniformity observed at 25 % w/v. Next, the influence of the print bed temperature was assessed by maintaining a polymer concentration of 25 % w/v and a printing speed of 15 mm/s, while varying the temperature to 30, 40, and 50 °C. Although temperature variation did not significantly alter pore distribution, a bed temperature of 50 °C was considered optimal to facilitate rapid solvent evaporation (Fig. 1b). The effect of printing speed was then examined by keeping the polymer concentration and bed temperature constant at 25 % w/v and 50 °C, respectively, while varying the speed to 5, 10, and 15 mm/s. Higher printing speeds were associated with improved scaffold pore uniformity (Fig. 1c), with the most uniform distribution achieved at 15 mm/s. Taken together, the optimal printing conditions for PCL scaffolds were determined to be a polymer concentration of 25 % w/v, a printing speed of 15 mm/s, and a receiving table temperature of 50 °C. Under these conditions, the SK content per unit area in the PCL/SK scaffold was $1.04 \pm 0.03\ \mu g/cm^2$. The PCL/SK scaffold showed a porous and breathable structure, which may be beneficial for healing of the diabetic wound.

The Fourier transform infrared spectroscopy (FTIR) spectrum of the PCL scaffold exhibited a characteristic bimodal peak at 2790–2950 cm^{-1}, corresponding to C–H stretching vibrations of methylene groups, and a prominent peak at 1725 cm^{-1}, attributed to carbonyl (C=O) stretching. The 700–1600 cm^{-1} region showed multiple bands associated with skeletal vibrations of the polymer chains. However, no distinct SK peaks were observed in the PCL/SK spectrum, likely due to its low loading (Fig. 1d). The crystal structures analyzed by X-ray diffraction (XRD) showed that the SK powder exhibited characteristic sharp diffraction peaks around 26° [22], indicating its crystalline nature. In contrast, PCL displayed distinct peaks at 21.3° and 24.1°, aligning with its semi-crystalline structure [23]. Notably, the PCL/SK scaffold did not exhibit the characteristic SK peaks (Fig. 1e), likely due to the low SK concentration. Furthermore, no discernible changes in peak position or shape were observed between PCL and PCL/SK. These results confirm that the addition of SK did not induce significant alterations in the crystalline structure of PCL. The results of the tensile strength of the PCL and PCL/SK scaffold materials revealed no significant difference, indicating that the incorporation of SK did not adversely impact the mechanical integrity of the PCL matrix (Fig. 1f). For the drug release study, PCL/SK scaffolds were placed in centrifuge tubes containing simulated physiological solution and incubated at 37 °C. As shown in Fig. 1g, the scaffolds exhibited a sustained release over 72 h, reaching a cumulative release of ~35 %.

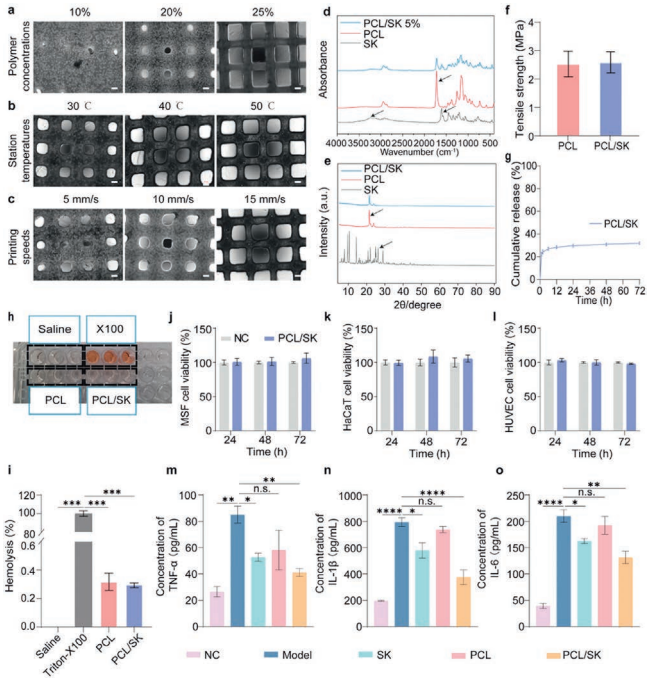


Fig. 1. Characterization and anti-inflammatory properties of PCL/SK scaffolds. Representative images of the scaffolds with different polymer concentrations (a), with different print bed temperatures (b), and with different printing speeds (c). Scale bar: 200 µm. (d) FTIR spectra. Arrows: main characteristic peaks. (e) XRD patterns. Arrows: main characteristic peaks. (f) Mechanical properties ($n = 3$). (g) The drug release curves for PCL/SK scaffolds. (h) Representative photograph of hemolysis assay. (i) Hemolysis of PCL/SK ($n = 3$). CCK-8 results of MSF (j), HaCaT (k), and HUVEC (l) treated with PCL/SK leaching solution at 24, 48, and 72 h. Expression levels of TNF-α (m), IL-1β (n), and IL-6 (o) measured by ELISA after incubation with PCL/SK leaching solution. Data are presented as mean ± SD. $^{*}P < 0.05$, $^{**}P < 0.01$, $^{***}P < 0.001$, $^{****}P < 0.0001$. n.s., not significant.

Blood compatibility of the scaffolds was evaluated using a hemolysis assay with the scaffold leachates. Both PCL and PCL/SK scaffolds exhibited hemolysis rates far below those caused by Triton-X100 and well under the 5 % threshold for hemolytic potential, confirming excellent blood compatibility (Figs. 1h and i). The biocompatibility of the PCL/SK scaffold was also assessed *in vitro* by incubation with mouse skin fibroblasts (MSF), human keratinocytes (HaCaT), and human umbilical vein endothelial cells (HUVEC). Cell viability was measured with the cell counting kit-8 (CCK-8) assay over 24–72 h. Leachates from both PCL and PCL/SK scaffolds showed no significant cytotoxicity compared to the negative control (NC) group across all cell types, indicating favorable biocompatibility (Figs. 1j–l).

RAW 264.7 cells were used to investigate the anti-inflammatory effects of the scaffolds. Lipopolysaccharide (LPS) served as a potent inducer of M1 polarization, and cytokine levels (tumor necrosis factor-alpha (TNF-α), interleukin-1β (IL-1β), and IL-6) were quantified using enzyme-linked immunosorben assay (ELISA). Compared with the NC group, the LPS group showed a marked increase

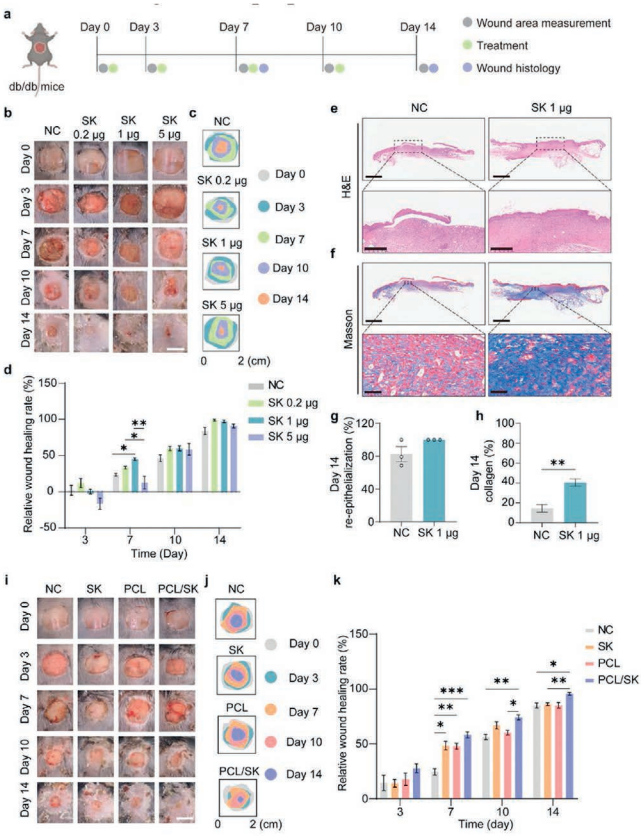


Fig. 2. Therapeutic effects of PCL/SK on the diabetic wound closure in *db/db* mice. (a) Schematic diagram of the diabetic wound model. (b) Representative images of the diabetic wounds on days 0, 3, 7, 10, and 14. Scale bar: 1 cm. (c) Traces of wound area for 14 days post-treatment. (d) Relative wound closure rate ($n = 4$). (e) H&E staining of wound tissues on day 14. Scale bars: 1250 μm (up), 400 μm (down). (f) Masson's trichrome staining of the wound bed on day 14. Scale bars: 1250 μm (up), 50 μm (down). (g) Re-epithelialization of wounds on day 14 ($n = 3$). (h) Collagen deposition of wounds on day 14 ($n = 3$). (i) Representative images of the diabetic wounds on days 0, 3, 7, 10, and 14. Scale bar: 1 cm. (j) Traces of wound area for 14 days post-treatment. (k) Relative wound closure rate ($n = 4$). Data are presented as mean ± SD. $^{*}P < 0.05$, $^{**}P < 0.01$, $^{***}P < 0.001$.

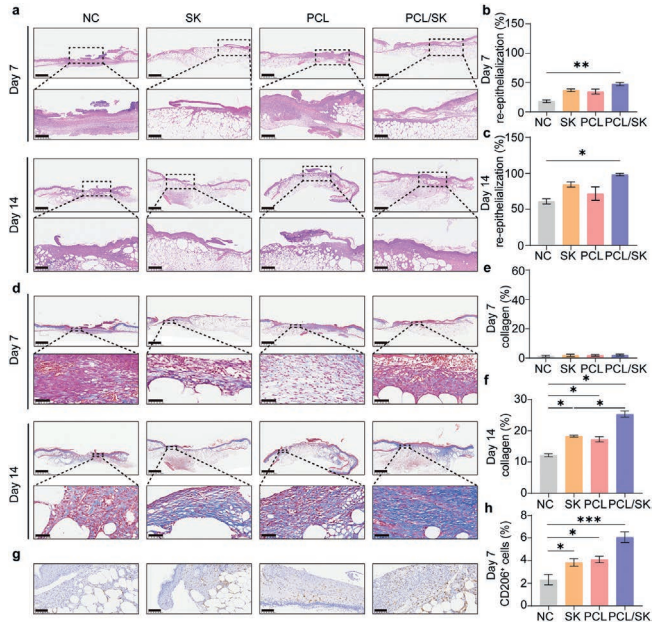


Fig. 3. Histopathological analysis of wound after different treatments. (a) H&E staining of wound tissues on day 7 and 14. Scale bars: 1250 μm (top), 400 μm (bottom). (b) Re-epithelialization of wounds on day 7 ($n = 3$). (c) Re-epithelialization of wounds on day 14 ($n = 3$). (d) Masson's trichrome staining of the wound bed on days 7 and 14. Scale bars: 1250 μm (top), 50 μm (bottom). (e) Collagen deposition of wounds on day 7 ($n = 3$). (f) Collagen deposition of wounds on day 14 ($n = 3$). (g) IHC staining of CD206 on day 7. Scale bar: 100 μm. (h) Quantitative analysis of $CD206^{+}$ IHC staining in the diabetic wound ($n = 3$). Data are presented as mean ± SD. $^{*}P < 0.05$, $^{**}P < 0.01$, $^{***}P < 0.001$.

in these pro-inflammatory cytokines, confirming successful induction of an inflammatory state. Notably, treatment with PCL/SK scaffolds significantly reduced TNF-α, IL-1β, and IL-6 levels relative to the LPS group (Figs. 1m–o). These findings indicate that the PCL/SK scaffolds possess anti-inflammatory properties and hold promise for wound healing applications.

To evaluate the therapeutic efficacy of PCL/SK scaffolds on diabetic wound repair, full-thickness dorsal wounds were established in *db/db* mice. All experimental procedures adhered to the protocols sanctioned by the Animal Ethics Committee of Nanjing University of Chinese Medicine (approval No. 202406A06). Wound areas were measured to calculate healing rates, and tissues were harvested for histopathological analysis on predetermined time point (Fig. 2a). Firstly, the therapeutic potential of SK in promoting diabetic wound healing was evaluated. Three concentrations (0.2, 1, and 5 μg/cm^2) were applied topically on days 0, 3, 7, and 10. Wound areas were recorded on days 0, 3, 7, 10, and 14 to calculate the healing rate. Statistical analysis revealed a dose-dependent effect on wound closure (Figs. 2b–d). Notably, the group receiving 5 μg/cm^2 SK group exhibited significantly delayed wound healing compared to 0.2 and 1 μg/cm^2 SK groups, potentially due to concentration-dependent cytotoxicity, consistent with the known anti-tumor activity of SK at elevated doses [24]. In contrast, the groups treated with 1 μg/cm^2 demonstrated significantly accelerated wound healing compared to the NC group by day 7 (Fig. 2d). The 1 μg/cm^2 dosage showed a more pronounced enhancement in repair compared to the 0.2 μg/cm^2 dosage. Consequently, the 1 μg/cm^2 concentration was selected for further investigation. Histological examination of wounds on day 14 using haematoxylin and eosin staining (H&E) staining confirmed complete re-epithelialization in the 1 μg/cm^2 SK group, with no significant difference compared to the NC group (Figs. 2e and g). Collagen deposition, a critical determinant of wound maturation, was quantified by Masson's trichrome staining. Compared to the NC group, the 1 μg/cm^2 SK group exhibited a significantly higher amount of collagen fiber proportion within the wound bed on day 14 (Figs. 2f and h).

Subsequently, the therapeutic efficacy of PCL/SK scaffolds in promoting diabetic wound healing was studied. Macroscopically, owing to PCL being an excellent support material and possessing sustained release and anti-inflammatory function, the PCL/SK scaffold group exhibited improved wound healing, with a wound healing rate of ~90 % on the 14th day, significantly higher than the NC group and SK group (Figs. 2i–k).

To verify the efficacy of the PCL/SK in diabetic wound healing, morphological analysis of wound site tissues harvested on day 7 and 14 was performed using H&E and Masson staining. H&E staining showed that the NC group had a large amount of inflammatory cell infiltration. After 14 days of treatment, the PCL/SK group exhibited reduced inflammatory cell and a significantly higher re-epithelialization rate (Figs. 3a–c). The generation of collagen plays a crucial role in the process of wound repair [25]. The collagen deposition in the wound bed was quantitatively analyzed using Masson staining. The results indicated no significant difference in collagen deposition between the PCL/SK scaffold group and other groups on day 7. This may be due to the early stage of wound healing of diabetic wounds and the collagen production in the wound bed is relatively low. By day 14 of treatment,

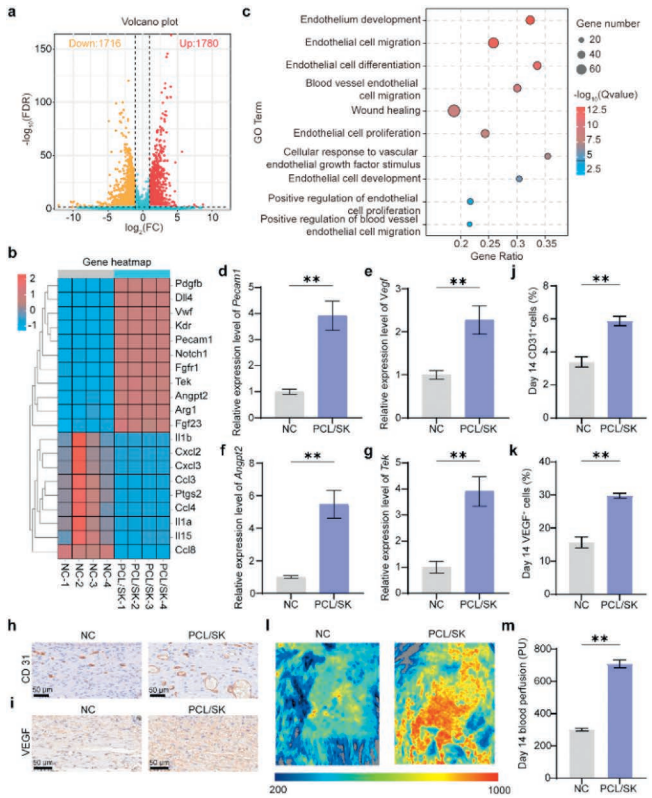


Fig. 4. Angiogenic function of PCL/SK scaffold in wounds. (a) Volcano plot. (b) Heatmap analysis of DEGs ($n = 4$). (c) Enriched GO functions of genes upregulated. (d–g) The mRNA expression of *Pecam1*, *Vegf*, *Angpt2*, and *Tek* on day 14. (h, i) IHC staining of CD31 and VEGF on day 14. Scale bar: 50 μm. (j, k) Quantitative analysis of $CD31^+$ and $VEGF^+$ IHC staining on day 14 ($n = 3$). (l) The laser Doppler perfusion imaging system of wound blood perfusion on day 14. (m) Blood perfusion in the wound on day 14 ($n = 3$). Data are presented as mean ± SD. $^{**}P < 0.01$.

compared with the control group, the collagen deposition density significantly increased in all treatment groups, among which PCL/SK scaffold group had the highest collagen deposition (Figs. 3d–f). Next, the immunohistochemistry (IHC) for anti-inflammatory factor CD206 was selected to further investigate the effect of the PCL/SK scaffold on inflammatory factors in diabetic wounds after treatment. The results showed that compared with the NC group, the PCL/SK scaffold group exhibited the highest number of $CD206^+$ cells. This suggests that the PCL/SK scaffold may enhance the release of anti-inflammatory factors in diabetic wounds (Figs. 3g and h). The H&E staining results of organs after 14 days of treatment confirmed that the PCL/SK scaffold exhibits good biocompatibility *in vivo* (Fig. S1 in Supporting information). These results indicated that PCL/SK could effectively eliminate wound inflammation, promote epithelial tissue regeneration and collagen deposition, and accelerate wound healing of diabetic wounds.

To investigate the potential mechanisms by which the PCL/SK scaffold facilitates wound repair in diabetic wounds, transcriptome sequencing was performed on the wound tissue after 14 days of treatment with PCL/SK. The volcano plots demonstrated the differential gene expression between the PCL/SK scaffold group and the NC group. We identified a total of 3496 differentially expressed genes (DEGs). Among these genes, 1780 showed upregulation in the PCL/SK scaffold group, while 1716 showed downregulation (Fig. 4a). The upregulated DEGs predominantly include genes associated with angiogenesis, such as platelet endothelial cell adhesion molecule 1 (*Pecam1*), vascular endothelial growth factor receptor (*Kdr*), angiopoietin 2 (*Angpt2*), and TEK receptor tyrosine kinase (*Tek*) (Fig. 4b). Conversely, the downregulated genes are primarily associated with inflammation, such as interleukin 1a (*Il1a*), interleukin 1b (*Il1b*), interleukin 15 (*Il15*), and prostaglandin endoperoxide synthase 2 (*Ptgs2*). These findings suggest that the PCL/SK scaffold may accelerate the healing of diabetic wounds by promoting angiogenesis and reducing inflammatory reaction.

Additionally, we conducted gene ontology (GO) enrichment analysis on all upregulated DEGs. The primary angiogenesis related functions enriched include endothelial development, endothelial cell migration, endothelial cell differentiation, vascular endothelial cell migration, wound repair, endothelial cell proliferation, cell response stimulated by vascular endothelial growth factors, endothelial cell development, positive regulation of endothelial cell proliferation, and positive regulation of vascular endothelial cell migration (Fig. 4c). These results indicate that the PCL/SK scaffold exerts a significant effect on angiogenesis.

To verify the role of PCL/SK in promoting angiogenesis during wound repair, the angiogenesis-related genes *Pecam1* [26], vascular endothelial growth factor (*Vegf*) [27], *Angpt2* [28], and *Tek* [29] were detected at the mRNA level. The results showed that, after 14 days of PCL/SK treatment, the gene expression levels of *Pecam1*, *Vegf*, *Angpt2*, and *Tek* were significantly elevated compared to those in the NC group (Figs. 4d–g). Furthermore, we analyzed the expression levels of CD31 and VEGF, which are commonly used as protein markers to assess angiogenic capacity [30,31], *via* IHC staining. The proportion of positive cells was subsequently quantified. The results indicated that the proportions of $CD31^+$ cells and $VEGF^+$ area in the PCL/SK scaffold group were approximately 1.8-fold higher than those in the NC group (Figs. 4h–k). These results confirm that the PCL/SK scaffold has a positive effect on promoting wound angiogenesis.

During wound healing, blood perfusion volume is a key indicator for assessing the progress of wound healing [32,33]. To further validate the angiogenic effect of PCL/SK scaffold, we measured the average blood flow perfusion in the wound using a blood flow meter. The results showed that PCL/SK treatment significantly enhanced wound blood flow perfusion, which was approximately 2.3 times higher than that in the NC group (Figs. 4l and m). This finding underscores the capacity of PCL/SK scaffold to promote angiogenesis during the wound healing process.

Diabetic wounds represent a significant public health challenge, adversely impacting individuals' health and quality of life. In this study, we introduce an innovative approach that synergistically combines TCM with biomaterials to develop a novel PCL/SK drug-loaded scaffold. This scaffold leverages the wound-healing properties of SK and the bacterial colony-regulating capabilities of PCL, aiming to enhance the healing of diabetic wounds.

Our findings indicate that a concentration of 1 μg/cm^2 of the scaffold yielded optimal healing outcomes for diabetic wounds, whereas a higher concentration of 5 μg/cm^2 impeded the wound repair process. This inhibitory effect at higher doses may be attributed to the anti-tumor properties of SK, which could induce cytotoxicity [34]. Histopathological analysis of the wound in the 1 μg/cm^2 group revealed superior re-epithelialization and collagen deposition.

Recent studies have demonstrated the versatility of 3D-printed PCL scaffolds as drug delivery systems for wound healing applications. For instance, an artificial skin patch fabricated *via* 3D printing using PCL, carboxymethyl chitosan, and curcumin exhibited both antimicrobial and regenerative functions [35]. Other active agents, such as metformin (Glucophage) [36] and juglone [37], have also been incorporated into PCL scaffolds, showing promising effects in promoting wound healing. Furthermore, by combining PCL with other polymers (*e.g.*, polyvinyl alcohol or chitosan), these scaffolds have been utilized to deliver various therapeutics including diltiazem [38], sildenafil [39], and the antibiotic amoxicillin [40]. Such composite systems allow precise control over drug

release kinetics and enable synergistic therapeutic outcomes. Collectively, these studies underscore that 3D-printed PCL scaffolds represent a highly adaptable platform capable of loading diverse drug molecules to meet specific therapeutic needs, thereby offering considerable potential for personalized treatment strategies.

While it is true that ideal 3D-printed scaffolds should possess good mechanical properties, degradability, and biocompatibility. Our selection of PCL was specifically driven by our preliminary research finding [41]. Previous research has established that PCL can modulate the wound microbiome, thereby accelerating wound healing [41]. Consequently, we integrated PCL with SK to fabricate the PCL/SK scaffold, selecting 1 μg/cm^2 as the optimal drug-loading capacity per unit area. The PCL/SK scaffold was subsequently characterized by FTIR, XRD, and mechanical properties assessment, among other techniques. The results showed no significant difference between both PCL/SK and PCL, indicating that the addition of SK did not affect the properties of PCL.

In vivo experimental results demonstrated that the PCL/SK scaffold group exhibited significantly enhanced wound healing effects on both day 7 and day 14. Concurrently, during the inflammatory phase of wound healing, CD206 IHC staining revealed that the PCL/SK scaffold group possessed the highest proportion of positive cells, suggesting its superior anti-inflammatory efficacy. This effect may be attributed to the synergistic action of PCL in modulating the wound microbiome, promoting the release of anti-inflammatory factors to accelerate healing [41], coupled with the inherent anti-inflammatory properties of SK [42]. Furthermore, transcriptome sequencing analysis demonstrated that following PCL/SK treatment, the differentially expressed upregulated genes and their associated GO functions were predominantly enriched in angiogenesis-related genes and functional pathways.

The critical role of angiogenesis in diabetic wound healing is substantial, as impaired neovascularization is a hallmark of diabetic ulcers, characterized by dysfunctional endothelial progenitor cells, reduced VEGF bioavailability, and persistent inflammation, which collectively compromise tissue perfusion and regenerative capacity [43]. Our findings demonstrate that PCL/SK treatment significantly upregulates angiogenesis-related genes and enriches associated GO functional pathways, as revealed by transcriptome sequencing. This provides a mechanistic explanation for the accelerated healing observed *in vivo*.

The synergy between PCL and SK appears to be crucial. While SK directly contributes to anti-inflammatory activity [42], PCL modulates the wound microbiome and promotes the secretion of anti-inflammatory factors [41], thereby creating a pro-regenerative microenvironment. This is further supported by the increased infiltration of CD206$^+$ macrophages in wounds treated with PCL/SK, indicating effective resolution of inflammation. Consequently, the enhanced vascular network may improve the delivery of oxygen and nutrients, sustain fibroblast proliferation, and support the maturation of granulation tissue, all of which are essential for overcoming the stagnation of healing in diabetic conditions.

Targeting angiogenesis thus represents a promising therapeutic approach for diabetic ulcers. Our findings position PCL/SK as a multifunctional scaffold that concurrently dampens inflammation and activates pro-angiogenic pathways, addressing key pathophysiological deficits. Future studies should validate the specific vascular mediators modulated by PCL/SK and assess the long-term microvascular density and functionality in diabetic models.

3D printing technology enables the personalized customization of wound dressings, allowing them to conform perfectly to irregular wound contours, an advantage unattainable with conventional dressings. Previous studies have incorporated antimicrobial metals such as zinc, copper, and silver into PCL to fabricate patient-specific dressings *via* 3D printing [44], highlighting its potential for precision medicine. Moreover, the integration of 3D printing with other techniques, such as electrospinning, has led to the development of biomimetic bilayer dressings [45] and skin substitutes loaded with human-derived keratin extracts [46], offering novel strategies to enhance wound repair.

However, several challenges remain. First, scalable production and quality control present significant hurdles; ensuring batch-to-batch consistency and stability of printed scaffolds is essential for industrialization. Second, although PCL is a Food and Drug Administration (FDA)-approved biodegradable material, the long-term biosafety of its degradation products and their effects within the complex diabetic microenvironment require further systematic evaluation. Finally, clinical validation is complicated by the high interpatient variability among diabetic wound cases. Well-designed, large-scale clinical trials are necessary to confirm the definite advantages of 3D-printed PCL scaffolds over existing standard treatments.

The clinical management of diabetic wounds remains a formidable challenge. TCM adheres to the principle of "personalized formulas based on syndrome differentiation" (bianzheng lunzhi), emphasizing individualized therapeutic strategies for treating diabetic wounds. The synergistic "TCM+biomaterial" design philosophy provides multimodal, multi-mechanistic precision healing strategies for wound repair. By integrating with the biomaterial PCL, *Lithospermum erythrorhizon*, a TCM herb known for its heat-clearing and blood-cooling properties, efficacy in the integrated treatment of TCM and Western medicine. This is achieved through a tripartite synergistic mechanism: regulation of the microbiome, inhibition of inflammation, and promotion of angiogenesis. The technical paradigm established in this study offers a versatile research platform for extending this approach to other topical Chinese herbs, particularly those with blood-cooling and blood-activating properties, in the context of diabetic wound repair. This advancement contributes significantly to enriching the theoretical framework and technical methodology of TCM external therapy.

In this study, we prepared PCL/SK scaffolds for the treatment of diabetic wound by combining SK, the active ingredient in TCM (*Lithospermum erythrorhizon*), with PCL using 3D printing technology. The scaffold formed accelerates the wound healing and showed good anti-inflammatory and angiogenic effects. These findings highlight the potential of combining traditional medicinal compounds with biomaterials to address the challenges of diabetic wound management. This study provides a novel technological platform for the development of multifunctional scaffolds and offers new insights into the integration of TCM with materials science for future therapeutic applications.

CRediT authorship contribution statement

Zeyu Xu: Writing – review & editing, Writing – original draft, Visualization, Methodology, Investigation, Formal analysis, Data curation, Conceptualization. **Ming Zhang:** Validation, Methodology, Investigation. **Tangtang He:** Investigation. **Zhe Wang:** Methodology. **Wenwen Deng:** Formal analysis. **Xia Cao:** Supervision. **Qilong Wang:** Supervision. **Yiwei Wang:** Funding acquisition. **Jun Chen:** Writing – review & editing, Funding acquisition.

Declaration of competing interest

The authors declare that they have no known competing financial interests or personal relationships that could have appeared to influence the work reported in this paper.

Acknowledgment

This work was supported by the National Natural Science Foundation of China (Nos. 82474200, 82372521).

Supplementary materials

Supplementary material associated with this article can be found, in the online version, at doi:10.1016/j.cclet.2025.112130.

References

[1] D.G. Armstrong, T.W. Tan, A.J.M. Boulton, et al., JAMa 330 (2023) 62–75.
[2] L. Xie, X. Zhang, X. Wang, et al., Chin. Chem. Lett. 36 (2025) 110848.
[3] S.A. Eming, P. Martin, M. Tomic-Canic, Sci. Transl. Med. 6 (2014) 265sr266.
[4] Y. Hong, Q. Su, X. Wu, et al., Chin. Chem. Lett. 37 (2026) 111846.
[5] J.G. Powers, C. Higham, K. Broussard, et al., J. Am. Acad. Dermatol. 74 (2016) 607–625.
[6] A.Y.W. Wong, N.M.F. Hooi, B.S.Y. Yeo, et al., J. Clin. Endocrinol. Metab. 109 (2024) e1642–e1651.
[7] Z. Xu, M. Dong, S. Yin, et al., Adv. Drug Deliv. Rev. 195 (2023) 114764.
[8] X. Zhou, S. Chen, B. Savitz, et al., Diabetes Obes. Metab. 27 (2025) 3431–3441.
[9] A.E. Louiselle, S.M. Niemiec, C. Zgheib, et al., Transl. Res. 236 (2021) 109–116.
[10] Y. Li, Z. Zhu, S. Li, et al., J. Nanobiotechnology 22 (2024) 398.
[11] M. Sharifiaghdam, E. Shaabani, R. Faridi-Majidi, et al., Mol. Ther. 30 (2022) 2891–2908.
[12] M. Rai, A. Yadav, A. Gade, Biotechnol. Adv. 27 (2009) 76–83.
[13] Y. Liang, Q. Li, L. Hu, et al., Chin. Chem. Lett. 35 (2024) 109459.
[14] B. Lu, D. Wang, J. Guo, et al., Chin. Chem. Lett. 36 (2025) 110601.
[15] Y. Liang, J. He, B. Guo, ACS Nano 15 (2021) 12687–12722.
[16] Z.U. Arif, M.Y. Khalid, R. Noroozi, et al., Int. J. Biol. Macromol. 218 (2022) 930–968.
[17] J. Xiao, X. Ai, C. Zhou, et al., Chin. Chem. Lett. 37 (2026) 111291.
[18] W. Huang, M. Lv, Z.G. Gao, Chin. Chem. Lett. 22 (2011) 749–752.
[19] A. Sadeghianmaryan, N. Ahmadian, S. Wheatley, et al., Int. J. Biol. Macromol. 266 (2024) 131207.
[20] C. Ding, J. Yang, N. Wang, et al., Int. J. Biol. Macromol. 262 (2024) 129937.
[21] C. Xue, J. Dou, S. Zhang, et al., J. Gene Med. 26 (2024) e3633.
[22] J. He, J. Incl. Phenom. Macrocycl. Chem. 63 (2008) 249–255.
[23] N. Joy, D. Venugopal, S. Samavedi, Eur. Polym. J. 168 (2022) 111102.
[24] C. Guo, J. He, X. Song, et al., Pharmacol. Res. 149 (2019) 104463.
[25] S. Sharma, V.K. Rai, R.K. Narang, et al., Life Sci. 290 (2022) 120096.
[26] B. Fuchs, S. Mert, D. Hofmann, et al., J. Tissue Eng. 16 (2025) 20417314251317542.
[27] G. Mao, S. Tian, Y. Shi, et al., Carbohydr. Polym. 311 (2023) 120757.
[28] L. Liu, X. Hao, J. Zhang, et al., Stem Cell Res. Ther. 15 (2024) 437.
[29] Y. Luo, X. Yi, T. Liang, et al., Stem Cell Res. Ther. 10 (2019) 279.
[30] Y. Hu, R. Tao, L. Chen, et al., J. Nanobiotechnology 19 (2021) 150.
[31] Z. Xu, G. Liu, P. Liu, et al., Acta Biomater. 147 (2022) 147–157.
[32] S. Li, J. Sun, J. Yang, et al., Biomater. Res. 27 (2023) 11.
[33] C.H. Su, W.P. Li, L.C. Tsao, et al., ACS Nano 13 (2019) 4290–4301.
[34] Y. Guo, M. Zhou, Z. Mu, et al., Biomed. Pharmacother. 165 (2023) 115138.
[35] T. Dong, R. Li, Z. Lu, et al., Int. J. Biol. Macromol. 318 (2025) 144844.
[36] S. Harmanci, A. Dutta, S. Cesur, et al., Polymers 14 (2022) 5306.
[37] M. Ayran, A.Y. Dirican, E. Saatcioglu, et al., Bioengineering 9 (2022) 427.
[38] M. Mehdikhani, P.Y. Huri, S.A. Poursamar, et al., Int. J. Biol. Macromol. 282 (2024) 136692.
[39] E.S. Rezaei, S.A. Poursamar, M. Naeimi, et al., Int. J. Biol. Macromol. 269 (2024) 131859.
[40] Y. Song, Q. Hu, S. Liu, et al., Int. J. Biol. Macromol. 275 (2024) 129705.
[41] Z. Xu, L. Zhang, Q. Tang, et al., Acta Pharm. Sin. B 15 (2025) 611–626.
[42] Y. Song, Q. Ding, Y. Hao, et al., Molecules 28 (2023) 7950.
[43] S.A. Eming, T.A. Wynn, P. Martin, Science 356 (2017) 1026–1030.
[44] Z. Muwaffak, A. Goyanes, V. Clark, et al., Int. J. Pharm. 527 (2017) 161–170.
[45] Z. Liu, X. Chen, C. Li, Biomed. Mater. 17 (2022) 055008.
[46] W.S. Choi, J.H. Kim, C.B. Ahn, et al., Polymers 13 (2021) 2584.